Astronomical and Astrophysical Transactions (*AApTr*), 2025, Vol. 35, Issue 4, pp. 361–378,
ISSN 1055-6796, Photocopying permitted by license only, ©Cambridge Scientific Publishers

Curvilinear approximation of interplanetary shock front

A.O. Shiryaev[1,*], K.B. Kaportseva[1,2], A.S. Lavrukhin[1]

[1] *Skobeltsyn Institute of Nuclear Physics, M.V. Lomonosov Moscow State University, Leninskie gory, GSP-1, Moscow, 119991 Russia*
[2] *Lomonosov Moscow State University, Faculty of Physics, Leninskie gory, GSP-1, Moscow, 119991 Russia*

Received 23 June, 2025; accepted 14 August, 2025

Interplanetary coronal mass ejections (ICMEs) are major solar plasma eruptions that propagate through the heliosphere into interplanetary space. Geoeffective ICMEs travel much faster than ambient solar wind, creating magnetohydrodynamic shockwaves. The geometry of the interplanetary shockwave affects the characteristics of the magnetospheric response. In this paper standard magnetohydrodynamic methods calculation of interplanetary shockwave normals are described and compared to multi-spacecraft kinematic methods. In addition to standard kinematic approximation via a plane we present a curvilinear model of the interplanetary shock front that models it as a section of the spherical surface. The use of curvilinear shock models can allow for more accurate estimation of the angle between the interplanetary shockwave normal and the Sun-Earth line, which affects the magnetospheric response. The results of magnetohydrodynamic and kinematic calculations of the geometry of the shock that caused the May 10, 2024 magnetic storm are presented and the obtained impact angle matches the results in established catalogs within 23 degrees.

Keywords: Shock waves, geomagnetic fields, space weather, shock geometry, coronal mass ejection, geomagnetic storm

1 Introduction

Solar activity phenomena, such as coronal mass ejections (CME) and coronal holes (CH), are sources of disturbed solar wind streams in the heliosphere – interplanetary coronal mass ejections (ICME) and stream/co-rotating interaction regions (SIR/CIR) respectively. These structures generally carry enhanced dynamic plasma pressure and are associated with shifted parameters of the interplanetary magnetic field (IMF) (Kilpua et al. 2017; Yermolaev et al. 2012). The interaction of the shock wave and its driver with Earth's magnetosphere leads to its rapid compression, efficient transfer

*Email: anton.o.shiryaev@gmail.com

of energy from the interplanetary medium to the magnetosphere, the development of ring currents and, ultimately, to geomagnetic storms. Shock waves are the first to interact with the magnetosphere, and their characteristics influence the pattern of geomagnetic response, as do the magnetic fields carried by the disturbed solar wind streams.

Interplanetary shocks are usually characterized by parameters such as their Mach number, ratios of various magnetohydrodynamic stream characteristics before and after the shock (called upstream and downstream values respectively), and the angle between the shock normal and the IMF vector θ_{Bn} (Hajra 2021; Zhou, Smith 2015; Pitňa et al. 2021). There are quasi-parallel and quasi-perpendicular shocks characterized by $\theta_{Bn} > 45°$ and $\theta_{Bn} < 45°$ respectively. Most shocks are quasi-perpendicular regardless of type of shock driver (Jurac et al. 2002). The analysis of structure and evolution of CME-driven shock waves by Pitňa et al. (2021) revealed that shock fronts typically exhibit a quasi-perpendicular geometry on average. However, upstream magnetic field fluctuations can locally modify the angle between the magnetic field and shock normal (θ_{Bn}), resulting in non-uniform shock fronts. Furthermore, the study found that CME-driven shocks demonstrate a transition from quasi-parallel to quasi-perpendicular geometry at larger heliocentric distances.

The angle between the shock normal and the Sun-Earth line, referred to as "impact angle", is also important for magnetosphere dynamics and is subject of intense study (Takeuchi et al. 2002; Wang et al. 2006; Oliveira, Raeder 2014; Samsonov et al. 2015; Oliveira, Raeder 2015; Oliveira, Samsonov 2018; Rudd et al. 2019). Oblique shocks were shown to produce slower and more asymmetric magnetospheric responses compared to frontal impacts. The studies demonstrate that, when other factors are equal, the inclination angle has a greater effect on the magnetospheric response than the shock speed itself. Front shocks produce rapid changes in magnetic indexes, otherwise inclined shocks tend to prolong sudden commencement (SSC) rise time and enhance spatial variations in geomagnetic disturbances.

The arrival of interplanetary shock waves affects multiple dynamic systems in the magnetosphere and its asymmetry. Previous studies (Samsonov et al. 2015; Oliveira et al. 2021) have shown that the change in the magnetic field on the Earth's surface will be more pronounced from the side (morning or evening) of the arrival of the interplanetary shock. MHD simulations (Selvakumaran et al. 2017) also highlight the significant effect of the shock impact angle on SSC time and the asymmetry of magnetospheric response. An investigation of the response of the auroral ionosphere to the shock wave that was registered on March 8, 2012 (Jin et al. 2016) has shown that ionospheric reaction occurs rapidly and is localized in the direction of the propagation of the shock wave. An analysis of high-latitude field-aligned current as measured by the AMPER (Active Magnetosphere and Planetary Electrodynamics Response Experiment) instrument (Shi et al. 2019) has shown that quasi-perpendicular shocks also produce more intense and sharper increase compared to inclined shocks. Therefore, understanding the geometry and dynamics of interplanetary shock waves in the solar wind – including shock front inclination and shock normal orientation – is crucial for elucidating the mechanisms behind geomagnetic storm development and for improving space weather forecasting.

The impact angle can differ for shocks driven by ICMEs and SIRs/CIRs. In cases where the source of the shock wave is an ICME, it is crucial whether the central or

peripheral part of the ICME interacts with Earth's magnetosphere. In a work that studied the features of geomagnetic disturbances depending on the region in which the ICME interacts with the magnetosphere (central, intermediate, peripheral) (Badruddin et al. 2019) it was shown that the strongest disturbances are caused by central impacts, and the DST recovery rate for such events is also greater. ICMEs interacting with the magnetosphere by their intermediate parts are characterized by longer SSC rise time and amplitude. This proves that shock driver geometry and trajectory influence shock front impact angle and, therefore, storm dynamics. Consequently the prediction and modeling of storm shape should be a way of improving the accuracy of space weather predictions, and efforts in this direction are already being made.

A study by Janvier et al. (2014) analyzed the average shape of interplanetary shock fronts at ≈ 1 AU using in situ data from L1 sattelites and STEREO-A/B spacecraft. The authors introduce a simple analytical model with a single free parameter λ – the angle between the shock normal and the radial direction from the Sun. The analysis shows that ICME-driven shock fronts are generally symmetric around the Sun-apex line, and observations agree well with this symmetric model, indicating a convex and elongated shock structure. In subsequent developments of this model, an ellipsoidal front with a fixed aspect ratio was introduced (Janvier et al. 2015), demonstrating the highest rates of coincidence with observed shock normals and magnetic cloud axes. Finally, in Perez-Alanis et al. (2023), this ellipsoidal shock model was applied to a multi-spacecraft dataset spanning from Mercury to Jupiter. The authors confirmed that the model remains consistent across heliocentric distances and found that the inferred shock front curvature increases with radial distance, supporting its use for large-scale heliospheric propagation studies.

In this work a curvilinear approach for modeling the shape of the interplanetary shock front is introduced and the results of the application of this approach to the interplanetary shock that preceded the May 10, 2024 magnetic storm are analyzed.

In Section 2 customary magnetohydrodynamic methods of shock normal estimation are reviewed and an overall approach to kinematic normal calculations is introduced. Planar and spherical kinematic models are specified and the spacecraft which registered the May 10, 2024 shock and will be used for shock normal calculation are listed. In Section 3 the May 10, 2024 event is briefly described and the shock normals obtained with the models described in Section 2 are presented. The results of curvilinear kinematic normal estimation are compared to established interplanetary shock catalogs. In Section 4 we summarize the research discussed and advantages, limitations and potential applications of the method.

2 Data and methods

2.1 Magnetohydrodynamic methods

Magnetohydrodynamic shock front modeling assumes that the shock front is a plane, and defines it by selecting two vectors of magnetic or plasma parameters that lie on the discontinuity plane. Several subsets of Rankine–Huginot relations (Kennel 1994) can be used to determine such vectors. The coplanarity theorem (Landau, Lifshitz 1984; Russell et al. 1983; Bykov et al. 2008) states that for a shockwave-type

discontinuity, the upstream and downstream magnetic field vectors $\mathbf{B}_u$ and $\mathbf{B}_d$, the upstream-to-downstream bulk velocity change vector $\Delta\mathbf{v}$ and the shock normal all lie in the same plane. There are multiple ways to express the shock normal from this theorem. A purely magnetic approximation ($\mathbf{n}_{MC}$, Colburn, Sonett 1966) uses only the upstream and downstream magnetic field and magnetic field change vectors to express the shock normal; however, it fails for highly oblique magnetic fields (Paschmann, Daly 1998). Somewhat similarly, a purely kinematic approximation ($\mathbf{n}_{VC}$, Abraham-Shrauner 1972) relies on the fact that it is possible to select a reference frame in which upstream and downstream bulk plasma velocity are coplanar to the shock normal vector; however, it is inapplicable at lower Alfvén Mach numbers when magnetic stresses are not negligible. Finally, there are mixed ($\mathbf{n}_{MX1}$-$\mathbf{n}_{MX3}$) (Paschmann, Daly 1998) methods which rely on both bulk velocity and magnetic field data. The equations of these methods are:

$$\mathbf{n}_{MC} = \frac{(\mathbf{B}_d \times \mathbf{B}_u) \times \Delta\mathbf{B}}{\|(\mathbf{B}_d \times \mathbf{B}_u) \times \Delta\mathbf{B}\|}, \tag{1}$$

$$\mathbf{n}_{MX1} = \frac{(\mathbf{B}_u \times \Delta\mathbf{v}^{arb}) \times \Delta\mathbf{B}}{\|(\mathbf{B}_u \times \Delta\mathbf{v}^{arb}) \times \Delta\mathbf{B}\|}, \tag{2}$$

$$\mathbf{n}_{MX1} = \frac{(\mathbf{B}_d \times \Delta\mathbf{v}^{arb}) \times \Delta\mathbf{B}}{\|(\mathbf{B}_d \times \Delta\mathbf{v}^{arb}) \times \Delta\mathbf{B}\|}, \tag{3}$$

$$\mathbf{n}_{MX3} = \frac{(\Delta\mathbf{B} \times \Delta\mathbf{v}^{arb}) \times \Delta\mathbf{B}}{\|(\Delta\mathbf{B} \times \Delta\mathbf{v}^{arb}) \times \Delta\mathbf{B}\|}, \tag{4}$$

$$\mathbf{n}_{VC} = \frac{(\mathbf{v}_d^{arb} - \mathbf{v}_u^{arb})}{\|(\mathbf{v}_d^{arb} - \mathbf{v}_u^{arb})|}, \tag{5}$$

where $\Delta\mathbf{B} = \mathbf{B}_u - \mathbf{B}_d$ and $\Delta\mathbf{v}^{arb} = \mathbf{v}_d^{arb} - \mathbf{v}_u^{arb}$. Indices u and d here refer to upstream and downstream vectors respectively, while *arb* indicates an arbitrary point of reference. The resulting normal can have either of two directions; while this affects calculations of its angle with, eg., the Earth–Sun line, when necessary the normal can be reversed trivially.

The upstream and downstream values for which the theorem is valid have to be obtained simultaneously; of course, such measurements are unobtainable in situ, and the data that is available is subject to significant turbulence. To reduce the effect of such noise on the result, various averaging methods are used. The simplest averaging method involves selecting "characteristic" upstream and downstream intervals of time and averaging over them to produce the upstream and downstream values required by the method. The shock analysis by Weiler (2025) uses 10 minute intervals and the Oliveira interplanetary shock database (Oliveira 2025) relies on five minute long intervals set five minutes before and after shock arrival time. It is important that the shock front itself is completely excluded from these averaging intervals (Paschmann, Daly 1998). However, the Larmor radius of protons in the solar wind is on the order of 100 km to 1000 km (Veselovsky et al. 2010; Malova et al. 2017), which at typical solar wind speeds is traversed in about a second. While the magnetic field averaging intervals we used to obtain normals vary by spacecraft and were chosen on a case-by-case basis to include "stable" upstream and downstream segments, they are generally

selected to be around 5 seconds away from the shock and 5 to 10 seconds long due to sufficiently high resolution.

The Center for Astrophysics (CfA) Interplanetary Shock Database (https://lweb.cfa.harvard.edu/shocks/) employs an alternative averaging method, where pairs of points are selected at random from the upstream and downstream regions and used to calculate a set of results, which are subsequently averaged. To apply further smoothing it is also possible to average the result of different magnetohydrodynamic expressions of the normal. For example, the Oliveira shock list averages three or more of the closest results out of the five possible (Oliveira, Raeder 2015) (three mixed magnetohydrodynamic expressions, purely solar wind velocity-based and purely magnetic) to produce the normals presented in the catalog. The abundance of smoothing methods indicates a crucial flaw of these methods – their results reflect the turbulent fine structures of solar wind and are strongly influenced by the specific choice of input data.

2.2 Kinematic methods

Kinematic modeling uses the time the shockwave took to traverse the distance between various spacecraft to project their locations into the same moment in time, yielding enough points to fully define a surface. These methods require data from multiple spacecraft that the shock has reached. Sometimes additional constraints have to be imposed on the plane in which the shock lies instead, like in Takeuchi et al. (2002), where only records from the Wind and IMP-8 spacecraft were available, which is not enough points to define an arbitrary plane. In contrast, more complex kinematic modeling becomes possible with the increasing number of spacecraft in orbit around L1 or when the shock was registered on satellites on near-Earth or near-Moon orbits.

These methods are obviously reliant on the determination of the shock velocity vector. There are established magnetohydrodynamic expressions for shock velocity based on plasma measurements (Paschmann, Daly 1998), but they are themselves expressed through the shock normal which cannot be obtained kinematically without knowing the shock velocity. When working with a planar shock model, a fourth spacecraft is used and the direction of the velocity is assumed to be that of the shock normal (Russell et al. 1983). However, with a curvilinear approach the normal obviously varies from point to point across the shock, so the question of shock velocity cannot be reduced to its magnitude. While further research into more accurate accounting for the direction and velocity of the shock's propagation is intended, in this paper the downstream ambient solar wind velocity is assumed to be sufficiently close to the shock propagation velocity to be used in its stead.

2.2.1 Surface

The simplest kinematic shock front model is a plane, which requires three spacecraft to define. Consider three spacecraft A, B and C, with position vectors $\mathbf{A}$, $\mathbf{B}$ and $\mathbf{C}$. The shockwave reaches these spacecraft at moments $t_{\mathbf{A}}$, $t_{\mathbf{B}}$, $t_{\mathbf{C}}$. Let's introduce $T_{AB} = t_{\mathbf{B}} - t_{\mathbf{A}}$ and $T_{AC} = t_{\mathbf{C}} - t_{\mathbf{A}}$. A plane can be expressed through its normal vector:

$$\mathbf{n} \cdot (\mathbf{R} - \mathbf{R_0}) = 0, \tag{6}$$

where $\mathbf{R}$ is the parameter and $\mathbf{R_0}$ is the position vector of a point that lines in the plane. At $t = T_{AB}$ a certain point of the shock had the position vector $\mathbf{B}$. We can use the velocity of the shock $\mathbf{v}$ and the time the shock took to propagate from spacecraft A to spacecraft B to obtain the coordinates of that point at $t = t_{\mathbf{A}}$:

$$\mathbf{B_A} = \mathbf{B} - \mathbf{v}\ T_{AB}. \tag{7}$$

Substitute $\mathbf{R}$ for this coordinate and $\mathbf{A}$ for $\mathbf{R_0}$ in Equation 6 to produce a condition for the normal vector n:

$$n \cdot (\mathbf{B} - \mathbf{v}\ T_{AB} - \mathbf{A}) = 0. \tag{8}$$

Since the spacecraft are ordered by shock arrival time, T_{AB} is positive, so the kinematic term has the negative sign. Performing the same projection for point $\mathbf{C}$ and time T_{AC} produces two equations. The normal vector is, by, definition, a unit vector, which is a condition we can use to yield a set of three equations for three components of n:

$$\begin{cases} n \cdot (\mathbf{B} - \mathbf{v}\ T_{AB} - \mathbf{A}) = 0 \\ n \cdot (\mathbf{C} - \mathbf{v}\ T_{AC} - \mathbf{A}) = 0 \\ |n| = 1\,. \end{cases} \tag{9}$$

Rather than solving a quadratic equation for three components, however, it is possible to use the collinearity of α $\mathbf{n}$ with $\mathbf{n}$ for any non-zero α to reduce the problem to a system of two linear equations by setting an arbitrary (non-zero) value for any component of $\mathbf{n}$, solving a system of the first two of equations 9 for the remaining two components and normalizing the resulting vector to obtain the normal. In fact, since the objective of shock normal calculation is to find of the direction of the shock, the normalization of $\mathbf{n}$ has purely symbolic value. Similarly to magnetohydrodynamic methods, it is possible to produce a shock normal of either direction. However, it is trivial to adjust the final result to match the direction of the shock's propagation.

The full expression of normal vector components will not be presented in this paper due to its verbosity, but can be obtained trivially with any computer algebra system.

It is important to note that this method is best applied to groups of spacecraft that are located so close that the curvature of the ICME front is not relevant. One example of such a group of spacecraft is ACE, Wind and DSCOVR, which oscillate around L1. Combining data from L1 spacecraft and data from spacecraft which are much farther away (such as STEREO-Ahead) is likely to produce inaccurate results.

2.2.2 Sphere

Magnetohydrodynamic modeling (Zhou, Feng 2021) shows that the ICME front demonstrates significant curvature at a magnitude of tens of Earth radii, which is comparable to the distances between spacecraft used for kinematic normal calculation. Therefore even a basic curvilinear model can significantly increase the accuracy of calculation of local shock normals. Curvilinear ICME shape approximations are also considered in works such as Janvier et al. (2014, 2015); Pérez-Alanis et al. (2023). The major limiting factor for such modeling is the limited number of spacecraft with high resolution magnetometer data that can be used to identify the exact moment of

a shock's passing. However, there are several satellites in selenocentric (THEMIS-B and THEMIS-C) or highly elliptical near-Earth orbits (such as CLUSTER or MMS) that, during part of their trajectory, operate in the interplanetary space ahead of the leading shock front. In cases of very significant geomagnetic storms the compression of Earth's magnetosphere can expose such satellites to the interplanetary shock (Fu et al. 2025; Weiler et al. 2025). The advantage of relying only on spacecraft located in L1 is the possibility of producing the shock impact angle approximately 30 minutes before it impacts Earth, which can be a sufficiently long period of time to be useful in space weather forecasting applications.

Since the shape of the ICME flux rope can by assumed to be cylindrical (Cargill 2004), it would be reasonable to approximate the shape of the shock wave cylindrically as well. However, as the objective of the methods described in this paper is the calculation of interplanetary shock geometry at scales comparable to those of the Earth's magnetosphere, a sphere has been chosen as the simplest surface that can account for the curvature of the shock front. A sphere only requires four points in space to define its position and radius, as opposed to five points necessary to define a cylinder. The general approach described here is adaptable to any surface in space, provided that data from a sufficient number of spacecraft is available.

It is important to note that we do not claim that the sphere in its entirety represents any physical shape of solar wind disturbance. Rather, a certain section of the surface limited by the projections of the locations of the spacecraft used to define the sphere represents the shock front. However, it is not unreasonable to assume that the shock extends some distance beyond these points. For example, it would not be inappropriate to extend the area of the sphere considered representative of the shockwave to include a point on the Sun–Earth line if all spacecraft used in the calculations lie on one side of it.

The equation set is constructed identically to the plane model. The equation that determines all points that lie on the surface of a sphere with center position vector $\mathbf{R_0}$ and radius r can be expressed in vector form as follows:

$$\|\mathbf{R} - \mathbf{R_0}\| = r, \tag{10}$$

where $\mathbf{R}$ is a point on the surface of the sphere. Substituting $\mathbf{R_0}$ in turn for $\mathbf{A}$, $\mathbf{B} - \mathbf{v}\ T_{AB}$, $\mathbf{C} - \mathbf{v}\ T_{AC}$ and $\mathbf{D} - \mathbf{v}\ T_{AD}$ produces a set of four equations with four unknowns (three components of the position vector $\mathbf{R_0}$ and radius r):

$$\begin{cases} \|\mathbf{A} - \mathbf{R_0}\| = r \\ \|\mathbf{B} - \mathbf{v}\ T_{AB} - \mathbf{R_0}\| = r \\ \|\mathbf{C} - \mathbf{v}\ T_{AC} - \mathbf{R_0}\| = r \\ \|\mathbf{D} - \mathbf{v}\ T_{AD} - \mathbf{R_0}\| = r\,. \end{cases} \tag{11}$$

To solve this set of equations it is best to express it in terms of vector components:

$$\begin{cases} (A_x - x_0)^2 + (A_y - y_0)^2 + (A_z - z_0)^2 = r^2 \\ (B_x - T_{AB}\ V_x - x_0)^2 + (B_y - T_{AB}\ v_y - y_0)^2 + (B_z - T_{AB}\ V_z - z_0)^2 = r^2 \\ (C_x - T_{AC}\ V_x - x_0)^2 + (C_y - T_{AC}\ v_y - y_0)^2 + (C_z - T_{AC}\ V_z - z_0)^2 = r^2 \\ (D_x - T_{AD}\ V_x - x_0)^2 + (D_y - T_{AD}\ v_y - y_0)^2 + (D_z - T_{AD}\ V_z - z_0)^2 = r^2, \end{cases} \tag{12}$$

where x_0, y_0 and z_0 are the components of $\mathbf{R_0}$. While this is technically a set of quadratic equations, it can be reduced to a set of linear equations for x_0, y_0, z_0 by subtracting the first equation from the other three. A further substitution of $\sigma = r^2$ makes the system fully linear and solvable instantaneously by any computer algebra system. The result of these steps and the full expression of the parameters of the sphere are omitted here for brevity.

2.3 Spacecraft used

Magnetohydrodynamic expressions of the shockwave normal rely on magnetic field and plasma data to express the shock normal, while kinematic methods rely on the coordinates of each spacecraft and the time it took for the shockwave to traverse the distance between them. Since the May 10, 2025 interplanetary shock had led to exceptional compression of the magnetosphere to around $5R_E$ (Fu et al. 2025), a wide variety of spacecraft were able to record the shock's parameters, including satellites that are typically positioned inside Earth's magnetosphere. Most commonly spacecraft in orbit around the L1 point are used to calculate magnetohydrodynamic shock normals. The spacecraft routinely used for this purpose are ACE, Wind and DSCOVR. SOHO, while also in such an orbit, is not equipped with a magnetometer, which limits the choice of magnetohydrodynamic model and makes it difficult to use kinematic methods accurately due to the comparatively lower resolution of solar wind velocity data. The Aditya-L1 spacecraft (Seetha, Megala 2017), launched in 2023, is equipped with two digital magnetometers and should be able to provide a fourth data point once open and real-time access to its coordinates and data is established. We also used data from the THEMIS-B satellite, which follows a selenocentric orbit, and MMS-1 on a close geocentric orbit.

Table 1 contains the resolutions of magnetic field vector, solar wind speed vector and spacecraft coordinate data used in our calculations. To work around the relatively lower resolution of solar wind data, when no data points fell into the averaging intervals used for magnetohydrodynamic calculations, we used the nearest data point available. Table 2 contains the coordinates of the spacecraft used for normal calculation and the time at which the shock had been registered on them.

Table 1 Resolution of spacecraft data used to calculate shock normals.

Spacecraft	Δt_B (s)	Δt_v (s)	Δt_R (s)
DSCOVR	1	20	720
ACE	1	≈60	720
Wind	1	≈60	720
THEMIS-B	5	1	60
MMS-1	1	5	60

Note: Δt_B is the resolution of the magnetic field vector data (in GSE); Δt_v, of the velocity vector, Δt_R, of the spacecraft coordinates.

Table 2 Shock time and spacecraft location data used for kinematic normal calculation.

Spacecraft	t_{shock}	GSE$_x$ (R_e)	GSE$_y$ (R_e)	GSE$_z$ (R_e)
DSCOVR	2024-05-10 16:35:10	244.55	–28.29	20.42
ACE	2024-05-10 16:37:03	223.81	3.00	22.36
Wind	2024-05-10 16:37:22	215.56	100.88	–1.02
THEMIS-B	2024-05-10 17:00:32	48.52	35.41	5.05
MMS-1	2024-05-10 17:04:04	11.59	–21.90	–6.59

3 Results and discussion

3.1 About the event

The methods described above have been applied to the ICME-driven interplanetary shock that led to the one of most intense geomagnetic storms ever observed. On May 11, 2024 the Dst geomagnetic index, which characterizes the axially symmetric disturbed magnetic field near the dipole equator on the Earth's surface, dropped below –400 nT, making it the 6th largest storm by Dst value since 1957 (Hayakawa et al. 2025). Sudden storm commencement rise time as indicated by the SYM-H index was around 7 minutes, which is greater than average (Takeuchi et al. 2002). In the first moments of this storm, geostationary satellites found themselves in the daytime magnetosheath, and then, at one point, even in interplanetary space, meaning the bow shock was located below the geostationary orbit (Tulasi Ram et al. n.d.). The magnetopause was compressed to $5R_E$ (Fu et al. 2025). A very strong asymmetry of the morning-evening magnetic field impulses was observed, as determined from SuperMAG indices SMR-06 and SMR-18 (Gjerloev 2012). These indices indicate the average values of axially symmetric magnetic field changes based on data from multiple stations located in the morning (06 LT) and evening (18 LT) sectors of the magnetosphere. The index of the magnetic field in the morning sector (SMR06) surged by 62.9 nT during the sudden storm commencement, and the index in the evening sector (SMR18) increased by 172.7 nT.

3.2 Normal calculation results

The averaging intervals for $\mathbf{B}_u$ and $\mathbf{B}_d$ estimation that were chosen for each spacecraft are presented in Figure 1 and the plasma speed and density data used to determine the moment the shock passed the spacecraft are in Figure 2.

The value for downstream solar wind velocity does not differ significantly between spacecraft. In kinematic calculations data from the ACE spacecraft has been used: $\mathbf{v}_x = -646$ km/s, $\mathbf{v}_y = -47$ km/s, $\mathbf{v}_z = 121$ km/s, for a speed value of $\|\mathbf{v}\| = 659$ km/s.

We have used the MX3 mixed method (eq. 4) for magnetohydrodynamic calculation of shock normals at DSCOVR, ACE, Wind, THEMIS-B and MMS-1 spacecraft. Both planar and spherical approximations of the shock normal front have been calculated. The DSCOVR, ACE and Wind spacecraft were used for planar approximation with the addition of Themis-B as the fourth data point for spherical approximation.

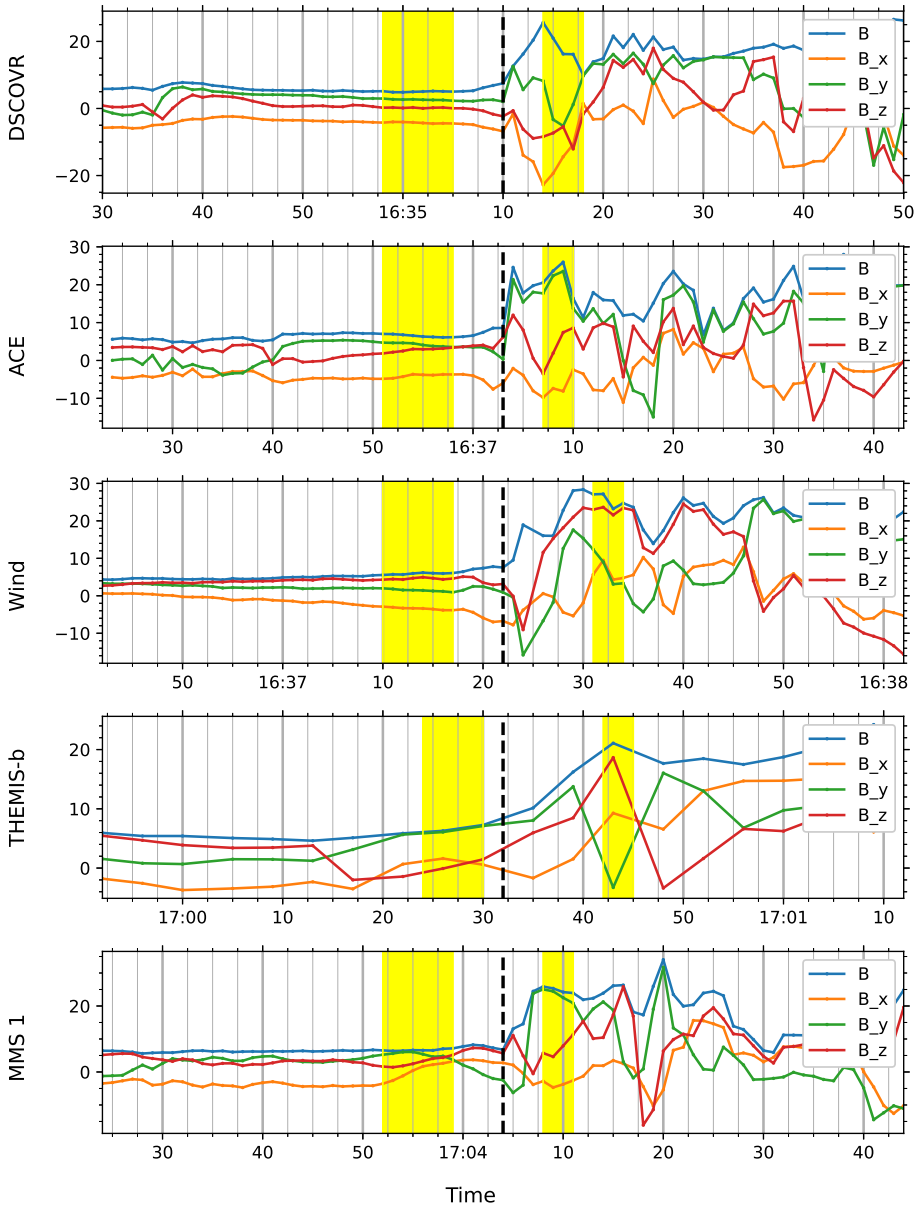


Figure 1 Magnetic field vector data used in magnetohydrodynamic calculations of shock normals. The vertical dashed line indicates the shock arrival time and the yellow rectangles indicate upstream and downstream averaging intervals. Note that each plot has its own x axis; they have been aligned by the shock arrival time.

Since the objective of normal calculation is typically discerning the inclination of the shock, various angles are more commonly used for analysis than the components of the normal vectors themselves. The values of shock impact angle (the angle the

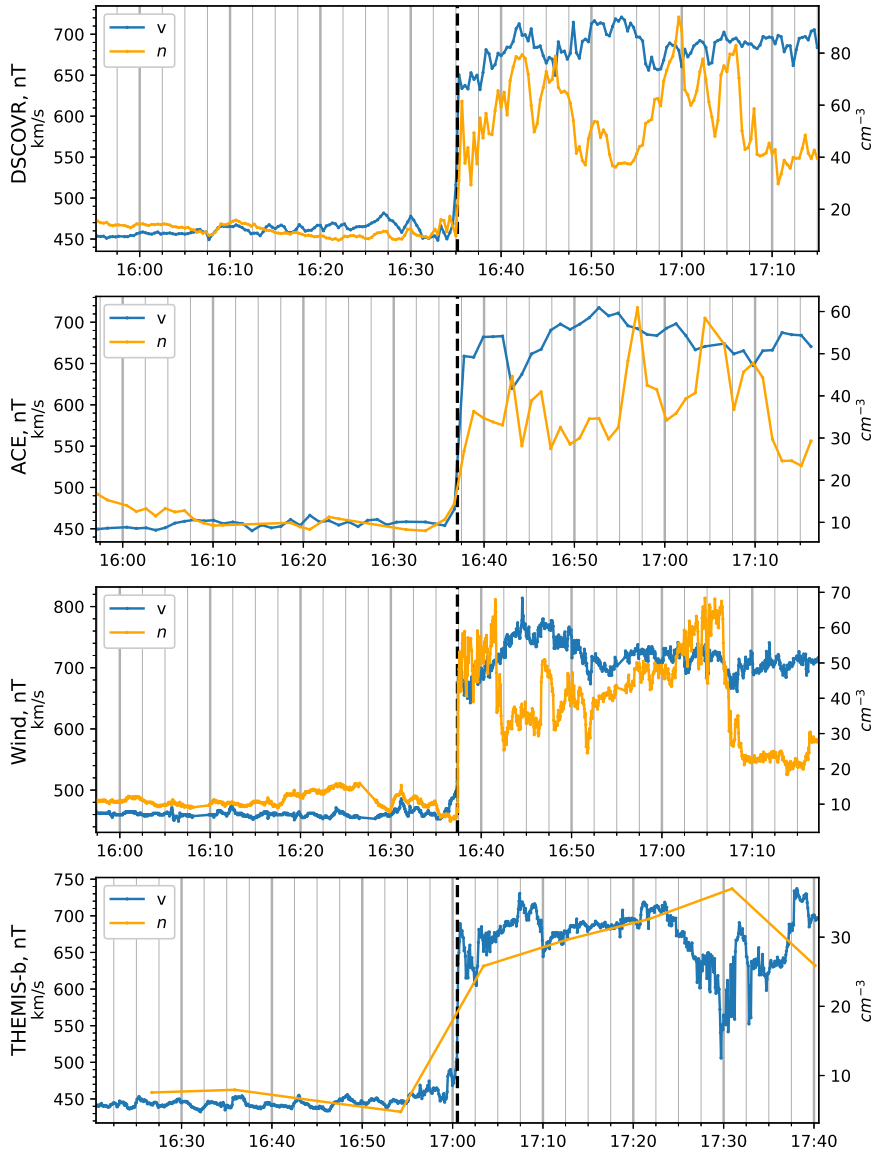


Figure 2 Density and bulk speed vector data used to determine the moment of a shock's passing. The vertical dashed line indicates the shock arrival time. The MMS-1 spacecraft has a gap in DIS-MOMS data from 06:00 to 18:00 UT, so magnetic field data has been used instead. Note that each plot has its own x axis; they have been aligned by the shock arrival time.

shock normal forms with the Sun–Earth line) and clock angle (the angle the shock normal's projection in YZ_{GSE} forms with the Y axis) obtained by various methods for various spacecraft are presented in Tables 3 and 4, respectively. The average difference

Table 3 θ_{X_n} (impact angle) values.

ϕ_{XY}	MX3	Sphere	Plane
DSCOVR	146.1°	131.5°	
ACE	144.6°	135.1°	
Wind	140.8°	137.6°	80.9°
THEMIS	164.2°	150.7°	
Sun–Earth line		157.1°	

Table 4 ϕ_{Y_n} (clock angle) values.

θ_{xz}	MX3	Sphere	Plane
DSCOVR	10.1°	22.3°	
ACE	34.5°	10.5°	
Wind	21.6°	31.1°	14.8°
THEMIS	3.9°	9.5°	
OX*		11.5°	

between magnetohydrodynamically and spherically obtained impact angles is 8.59° and the average clock angle difference is 12.44°. The projections of local tangents to the shock to XY_{GSE} and XZ_{GSE} planes are presented in Figure 3. The dotted lines indicate magnetohydrodynamic results, the dashed line indicates the projection of the kinematically obtained surface. The sphere has been intersected with the planes XY_{GSE} and XZ_{GSE} at the moment when its surface passed the DSCOVR spacecraft. A three-dimensional representation of the sphere produced via the curvilinear model approximation method is presented in Figure 4.

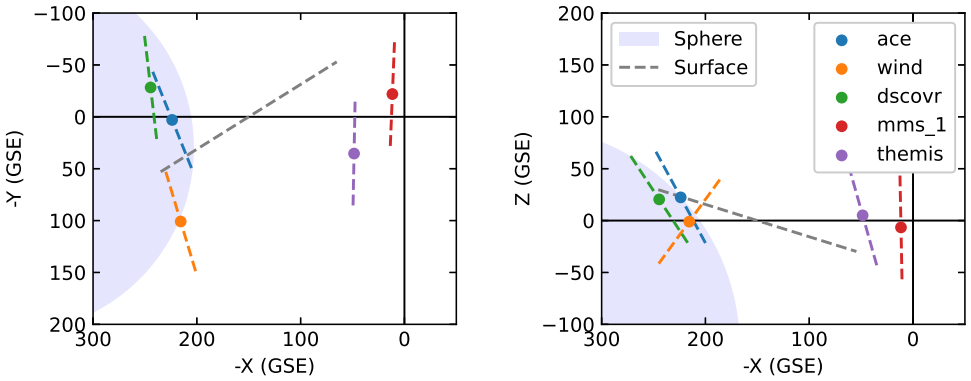


Figure 3 Shock normal calculation results. Dashed lines indicate magnetohydrodynamically obtained local normals; the dotted line, the result of kinematic approximation with a plane and the circles are the intersections of the sphere produced by curvilinear normal approximation into XY and XZ planes. All coordinates are given in Earth radii in GSE. Note that the directions of X and Y have been inverted to match directions used in GSFC satellite locator plots.

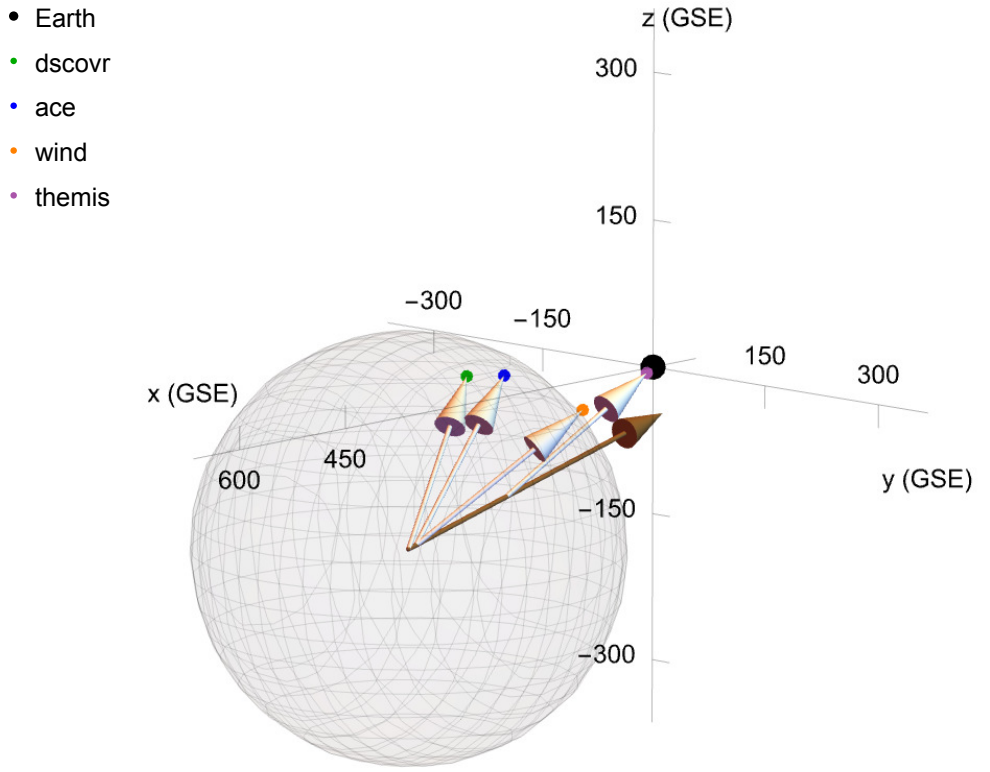


Figure 4 The sphere obtained with the curvlinear shock determination algorithm at the point it passed DSCOVR and shock normals obtained with it for DSCOVR, ACE, Wind and THEMIS-B. The light arrows indicate local shock normals and the brown arrow denotes the direction of the propagation of downstream solar wind. All coordinates are in Earth radii.

3.3 Comparison with other catalogs and Discussion

Some significant discrepancies in the obtained normals need to be noted. Magnetohydrodynamically produced normals are mostly in agreement between spacecraft, except those calculated for the Wind spacecraft. This can be explained both by inaccuracies in the data, the averaging process or the method; and by the fact that the Wind spacecraft was the furthermost from the Sun-Earth line. However, as we have noted in Section 2, the result of magnetohydrodynamic shock normal calculation is highly dependent on the averaging method. The planar kinematic model has yielded an extremely inclined result in both XY and XZ planes of the geocentric solar ecliptic coordinate system. The spherical model has produced results mostly similar to the magnetohydrodynamic ones, with the exception, again, of the Wind spacecraft.

We have compared our results with shock normals presented by the Oliveira (Oliveira 2025) and Harvard CfA interplanetary shock lists. When working with the CfA list, we have selected MX3 values for comparison.

A comparison of impact angle values is presented in Table 5. An impact angle value of 180° would correspond to a fully frontal shock. The impact angle obtained spherically for the DSCOVR spacecraft is 131.5°, while the Oliveira catalog proposes 145.2°. The local normal at the Wind spacecraft demonstrated an impact angle of 140.8° according to the spherical model and 169.8° according to the CfA catalog. Despite the 21.4° average difference between our results and established catalogs, all values indicate a somewhat inclined shock.

Table 5 Comparison of impact angle values with Oliveira and CfA catalogs.

	MX3	Sphere	Oliveira	CfA (MX3)
DSCOVR	146.1°	131.5°	145.2°	
Wind	140.8°	137.6°		169.8°

Clock angle is less frequently analyzed, but can be used to predict North–South and East–West asymmetries in the magnetospheric response. The average difference between spherical results and results presented by Oliveira or CfA is 22.9°. A detailed comparison of values is presented in Table 6.

Table 6 Comparison of clock angle values with Oliveira and CfA catalogs.

	MX3	Sphere	Oliveira	CfA (MX3)
DSCOVR	10.1°	22.3°	0.2°	
Wind	21.6°	31.1°		7.44°

The angle between the shock normal at the Wind spacecraft obtained via spherical approximation and the angle presented in the CfA list based on Wind data is 50.7°. The angle between the spherically obtained normal at DSCOVR and the normal from the Oliveira list is 20.1°.

Figure 5 presents the normal vectors obtained magnetohydrodynamically and spherically in this work with those from the CfA and Oliveira catalogs.

4 Conclusions

In this work we discuss different methods for calculating shock normals. magnetohydrodynamic (MHD) methods have been well studied and used for decades, but they are reliant on the assumption of a pl. Data from different spacecraft can vary significantly, and the choice of data averaging techniques can strongly affect the results.

On the other hand, the kinematic method makes it possible to reconstruct the shock front geometry based on the positions of multiple spacecraft. The main limitation of this approach is that it requires measurements from at least three spacecraft, or four to take into account the difference between shock speed and downstream solar wind speed. Fortunately, modern missions provide sufficient data coverage: measurements from ACE, Wind, and DSCOVR are reliably available, and Faraday cup data from SOHO can also be used when necessary. Since 2023, partial data from the Aditya-L1 spacecraft have also become accessible, meaning we now have up to 5

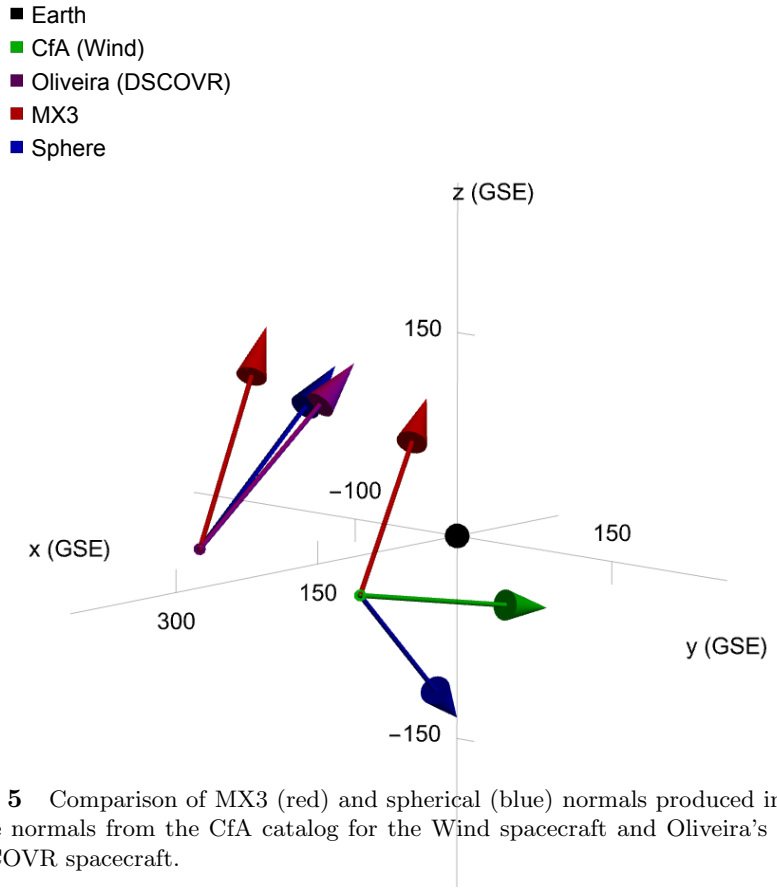


Figure 5 Comparison of MX3 (red) and spherical (blue) normals produced in this work with the normals from the CfA catalog for the Wind spacecraft and Oliveira's catalog for the DSCOVR spacecraft.

observation points at the L1 Lagrange point, which allows for short-term forecasting of shock front arrival and inclination. Additionally, a large number of near-Earth and some lunar-orbiting spacecraft equipped with magnetometers have become accessible, further expanding observational capabilities in cases of severe geomagnetic storms.

A key advantage of the kinematic method is its stability, which it retains even in cases of strong downstream magnetic field fluctuations. In contrast to MHD-based approaches, this method does not require precise measurements of downstream magnetic field components or plasma velocity – only the timing of disturbance detection at each spacecraft and their coordinates. Another benefit is that, also unlike mixed MHD methods, the kinematic approach does not require simultaneous measurements of both magnetic field and plasma velocity. Access to a single time series of any parameter sensitive to shock propagation, such as only the magnetic field or only the solar wind speed, is sufficient to determine the moment of a shock's arrival. This is especially useful when dealing with data where some instruments suffer gaps during the shock's passage.

In this paper a spherical kinematic approximation method is presented and compared to well-established magnetohydrodynamic methods. These models are evaluated on the interplanetary shock that caused the May 10, 2024 geomagnetic storm.

The conclusions based on the curvilinear model, on average, differ from those of magnetohydrodynamic methods by 8.59° for the impact angle and 12.43° for the clock angle. This discrepancy is comparable to the difference between various magnetohydrodynamic methods – for example, the mean difference between impact angles of normals obtained via MX3 and other magnetohydrodynamic methods presented in the CfA catalog is 35.8°.

The kinematic method can also be extended to different geometric approximations, which we plan to explore in future work. Accounting for the shock velocity remains an important problem. Adaptation of mixed MHD-kinematic methods, as described by Russel and Mellot (Russell et al. 1983), to curvilinear models is one potential avenue towards assessing shock velocity without introducing three more spacecraft to define it kinematically. Additionally, it is possible to consider shock front expansion when modeling the shock's evolution over significant distances. An investigation into which of the array of approximations or methods produce the best results for shocks caused by different sources, such as SIRs/CIRs and CMEs, could be the subject of future work.

By refining the approach described in this paper, we can improve the accuracy of shock parameter evaluation and enhance space weather forecasting.

Acknowledgements

This work has made use of data from the Satellite Situation Center of the NASA Goddard Space Flight Center (https://sscweb.gsfc.nasa.gov/) for spacecraft coordinates, trajectories and data, the PySPEDAS interface for SPEDAS (Space Physics Environment Data Analysis System) (https://spedas.org (Angelopoulos et al. 2024)) for spacecraft data access, the Harvard Center for Astrophysics Interplanetary Shock Database (https://lweb.cfa.harvard.edu/shocks/) and the Oliveira interplanetary shock database (https://zenodo.org/records/15121223 (Oliveira 2025)) for validation of shock calculation results. We gratefully acknowledge the SuperMAG collaborators (https://supermag.jhuapl.edu/info/?page=acknowledgement) (Gjerloev 2012).

The study was conducted under the state assignment of Lomonosov Moscow State University.

References

A. Bykov, K. Dolag, F. Durret (2008) *Space Science Reviews* 134 doi: 10.1007/s11214-008-9312-9.

Abraham-Shrauner, Barbara (1972) *Journal of Geophysical Research* 77, 4, 736 doi: 10.1029/JA077i004p00736.

Angelopoulos, Vassilis, Jim Lewis, James McTiernan, et al. (2024), https://zenodo.org/records/15023025 doi: 10.5281/zenodo.15023025.

Badruddin, A. Kumar, M. Derouich (2019) *Astrophysics and Space Science* 364, 4 doi: 10.1007/s10509-019-3560-x.

Cargill, Peter J. (2004).

Colburn, D.S., C.P. Sonett (1966) *Space Science Rev.* 5, 4 doi: 10.1007/BF00240575.
Fu, W. D., H. S. Fu, W. Z. Zhang, et al. (2025) *Geophysical Research Letters* 52, 5, e2024GL114040 doi: 10.1029/2024GL114040.
Gjerloev, J. W. (2012) *Journal of Geophysical Research: Space Physics* 117, A9 doi: 10.1029/2012JA017683.
Hajra, Rajkumar (2021) *The Astrophysical Journal* 917, 2, 91 doi: 10.3847/ 1538-4357/ac0897.
Hayakawa, Hisashi, Yusuke Ebihara, Alexander Mishev, et al. (2025) *The Astrophysical Journal* 979, 1, 49 doi: 10.3847/1538-4357/ad9335.
Janvier, M., S. Dasso, P. Démoulin, et al. (2015) *Journal of Geophysical Research: Space Physics* 120, 5, 3328 doi: 10.1002/2014JA020836.
Janvier, M., P. Démoulin, S. Dasso (2014) *Astronomy & Astrophysics* 565, A99 doi: 10.1051/0004-6361/201423450.
Jin, Yaqi, Jøran I. Moen, Wojciech J. Miloch, et al. (2016) *Journal of Geophysical Research: Space Physics* 121, 5, 4679 doi: 10.1002/2016JA022613.
Jurac, S., J. C. Kasper, J. D. Richardson, et al. (2002) *Geophysical Research Letters* 29, 10 doi: 10.1029/2001GL014034.
Kennel, Charles F. (1994) vol. 314, 180 doi: 10.1063/1.46750.
Kilpua, E. K. J., A. Balogh, R. Von Steiger, et al. (2017) *Space Science Reviews* 212, 3–4, 1271 doi: 10.1007/s11214-017-0411-3.
Landau, L.D., E.M. Lifshitz (1984) "MAGNETOHYDRODYNAMICS" in: *Electrodynamics of Continuous Media* Elsevier, 225 isbn: 978-0-08-030275-1 doi: 10.1016/B978-0-08-030275-1.50014-X https://linkinghub.elsevier.com/retrieve/pii/B9780080302751500 14X (visited on 08/08/2025).
Malova, H. V., V. Yu. Popov, E. E. Grigorenko, et al. (2017) *The Astrophysical Journal* 834, 1, 34 doi: 10.3847/1538-4357/834/1/34.
Oliveira, D. M., J. Raeder (2014) *Journal of Geophysical Research: Space Physics* 119, 10, 8188 doi: 10.1002/2014JA020275.
Oliveira, D.M., A.A. Samsonov (2018) *Advances in Space Research* 61, 1, 1 doi: 10.1016/j.asr.2017.10.006.
Oliveira, Denny M. (2025), https://zenodo.org/records/15121223 doi: 10.5281/zenodo.15121223.
Oliveira, Denny M., Joachim Raeder (2015) *Journal of Geophysical Research: Space Physics* 120, 6, 4313 doi: 10.1002/2015JA021147.
Oliveira, Denny M., James M. Weygand, Eftyhia Zesta, et al. (2021) *Space Weather* 19, 12, e2021SW002933 doi: 10.1029/2021SW002933.
Paschmann, G., Patrick W. Daly (1998) *ESA Publications Division* www.issi.unibe.ch.
Pérez-Alanis, Carlos Arturo, Miho Janvier, Teresa Nieves-Chinchilla, et al. (2023) *Solar Physics* 298, 4, 60 doi: 10.1007/s11207-023-02152-3.
Pitňa, A., J. Šafránková, Z. Němeček, et al. (2021) *Frontiers in Physics* 8, 626768 doi: 10.3389/fphy.2020.626768.
Rudd, J.T., D.M. Oliveira, A. Bhaskar, et al. (2019) *Advances in Space Research* 63, 1, 317 doi: 10.1016/j.asr.2018.09.013.
Russell, C. T., M. M. Mellott, E. J. Smith, et al. (1983) *Journal of Geophysical Research: Space Physics* 88, A6, 4739 doi: 10.1029/JA088iA06p04739.
Samsonov, A. A., V. A. Sergeev, M. M. Kuznetsova, et al. (2015) *Geophysical Research Letters* 42, 12, 4716 doi: 10.1002/2015GL064294.

Seetha, S., S. Megala (2017) *Current Science* 113, 04, 610 doi: 10.18520/cs/v113/i04/610-612.

Selvakumaran, R., B. Veenadhari, Y. Ebihara, et al. (2017) *Advances in Space Research* 59, 5, 1425 doi: 10.1016/j.asr.2016.12.010.

Shi, Yining, Denny M. Oliveira, Delores J. Knipp, et al. (2019) *Space Weather* 17, 12, 1659 doi: 10.1029/2019SW002367.

Takeuchi, T., C. T. Russell, T. Araki (2002) *Journal of Geophysical Research: Space Physics* 107, A12, p. SMP 6–1-SMP 6 doi: 10.1029/2002JA009597.

Tulasi Ram, S., B. Veenadhari, A. P. Dimri, et al. (n.d.) 22.

Veselovsky, I. S., A. V. Dmitriev, A. V. Suvorova (2010) *Cosmic Research* 48, 2, 113 doi: 10.1134/S0010952510020012.

Wang, C., C. X. Li, Z. H. Huang, et al. (2006) *Geophysical Research Letters* 33, 14, 2006GL025966 doi: 10.1029/2006GL025966.

Weiler, E., C. Mostl, E. E. Davies, et al. (2025) *Space Weather* 23, 3, e2024SW004260 doi: 10.1029/2024SW004260.

Yermolaev, Y. I., N. S. Nikolaeva, I. G. Lodkina, et al. (2012) *Journal of Geophysical Research: Space Physics* 117, A9, 2011JA017139 doi: 10. 1029/2011JA017139.

Zhou, Xiaoyan, Edward J. Smith (2015) *Journal of Geophysical Research: Space Physics* 120, 3, 1526 doi: 10.1002/2014JA020700.

Zhou, Yufen, Xueshang Feng (2021) *Universe* 7, 11, 431 doi:10.3390/universe7110431.